New Euclidean axion wormholes

George Lavrelashvili

A.Razmadze Mathematical Institute
at I.Javakhishvili Tbilisi State University

Based on Phys Rev D, 2023 with Jonas & Lehners
& earlier results with Rubakov & Tinyakov

Yerevan, October 2, 2023

Plan

- 1. Introduction
- 1.1 Remark I: 3 types of Euclidean solutions
- 1.2 Remark II: Topology fluctuations/wormholes
- 1.3 Remark III: Baby universe interpretation
- 1.4 Remark IV: linear stability analysis
- 2. Our setup
- 3. Axion wormholes with massive dilaton
- 4. Axion wormholes with scalar field
- 5. Concluding remarks

I. Euclidean solutions: Instantons in gauge theory

Belavin, Polyakov, Schwartz, Typkin ‘75

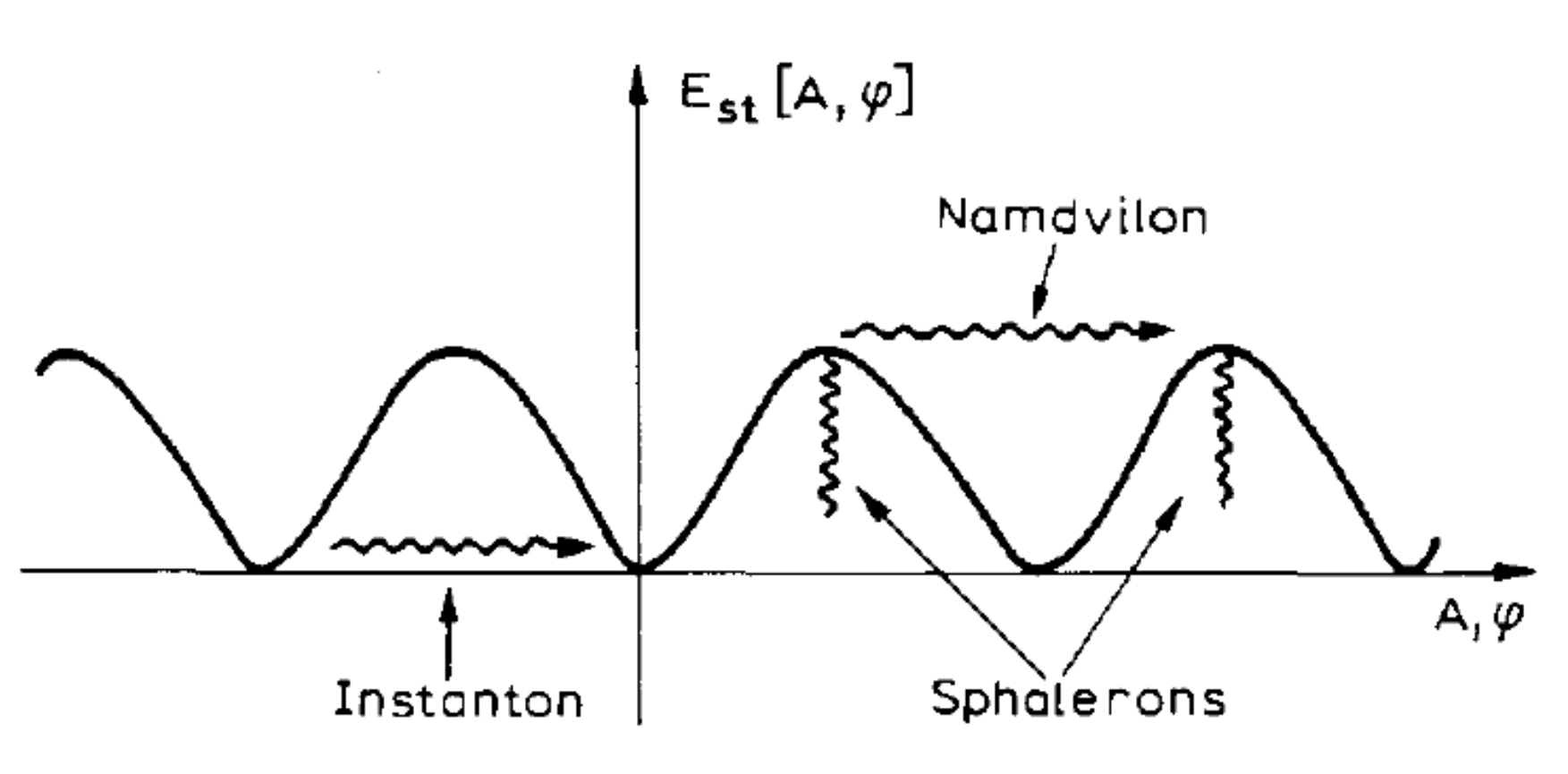

I. Euclidean solutions: Instantons in double well

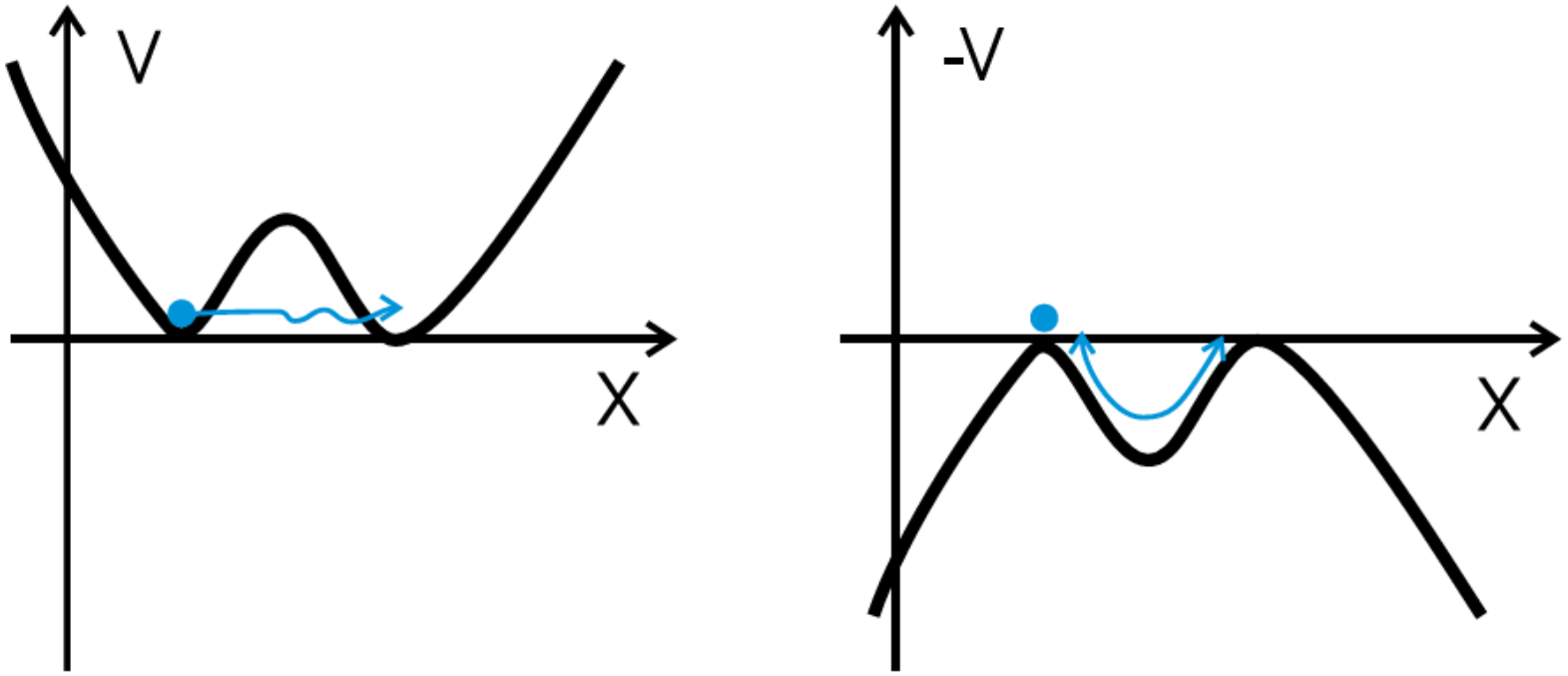

Figure 1: Tunneling in symmetric double well potential.

$$E = E_0 \pm \Delta E, \quad \Delta E = A\ \mathrm{e}^{-S[\mathrm{instanton}]}$$

I. Euclidean solutions: Bounce in asymmetric double well

Coleman 1977

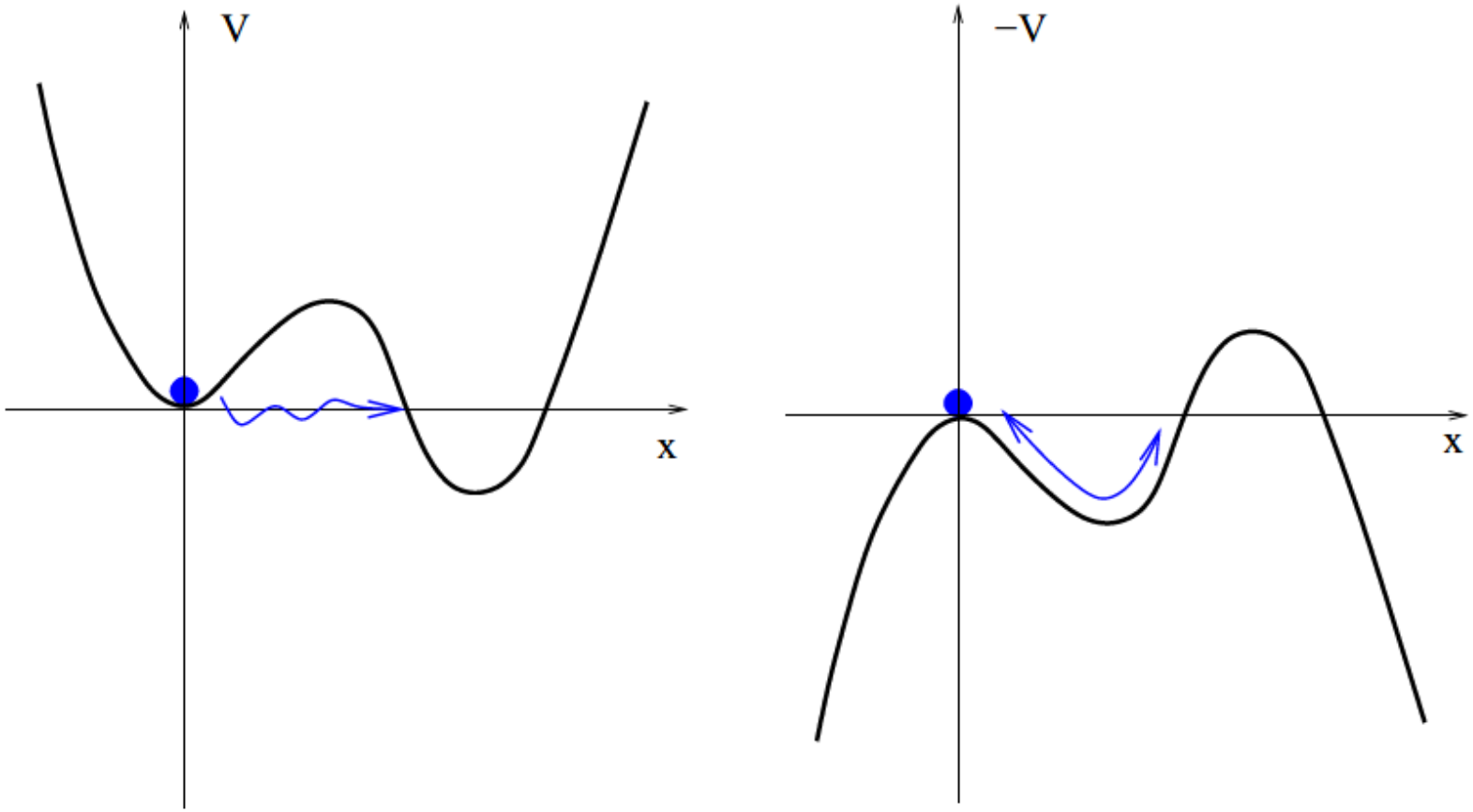

$$E = E_0 + i\Gamma, \quad \Gamma = A\, e^{-S[\text{bounce}]}$$

I. Euclidean solutions: Oscillating bounces

Coleman, De Luccia 1980,
Hackworth, Weinberg, 2004

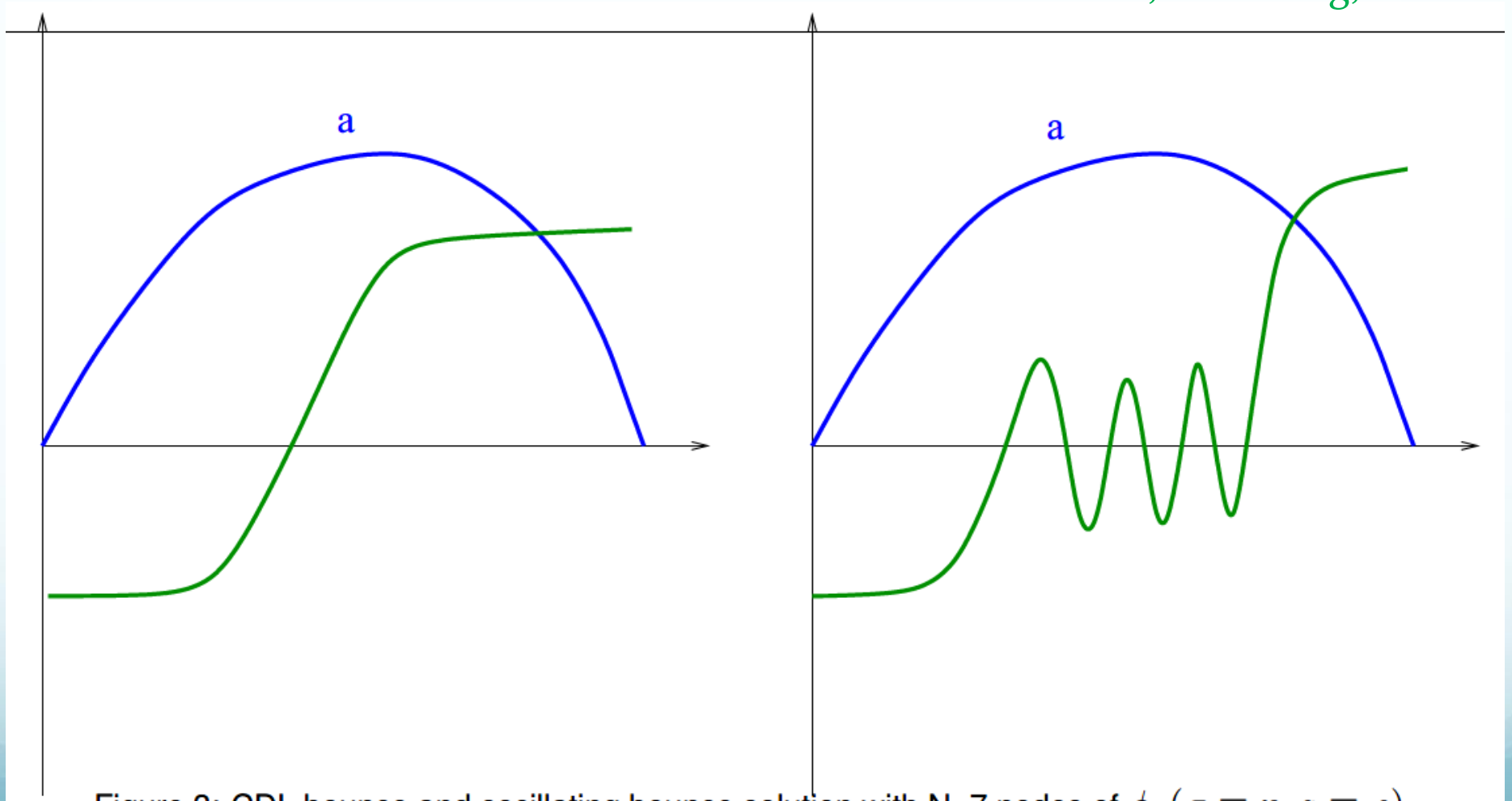

Figure 3: CDL bounce and oscillating bounce solution with N=7 nodes of ϕ, $(\sigma \equiv \eta, a \equiv \rho)$.

II. Fluctuations of Topology

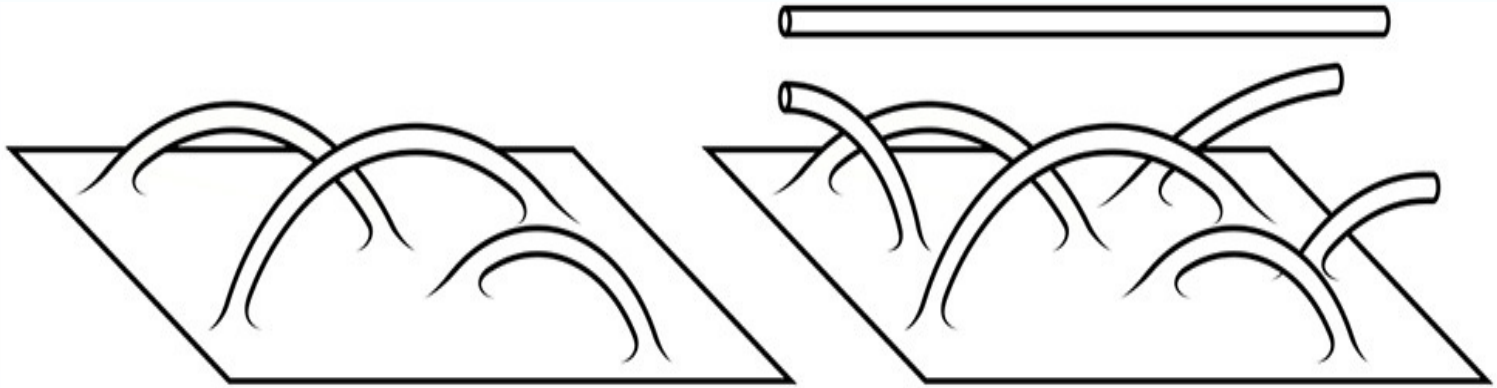

II. Transitions with change of topology & particle creation

G.L., Rubakov, Tinyakov (1987)

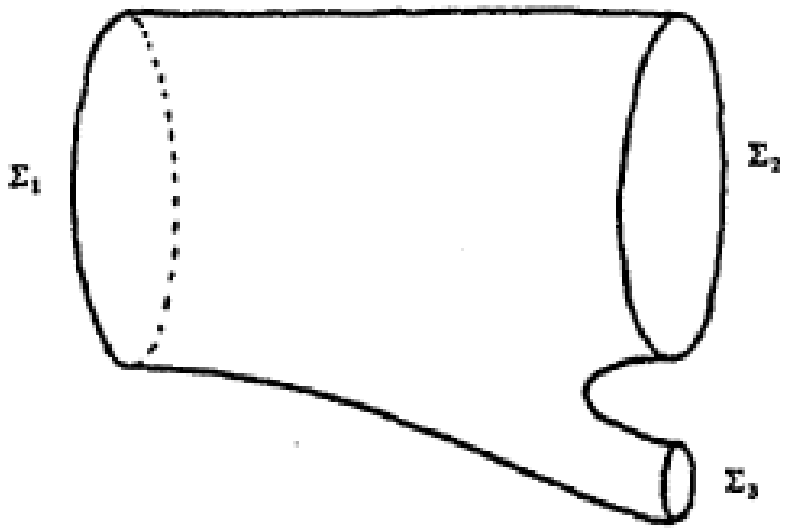

Fig. 1

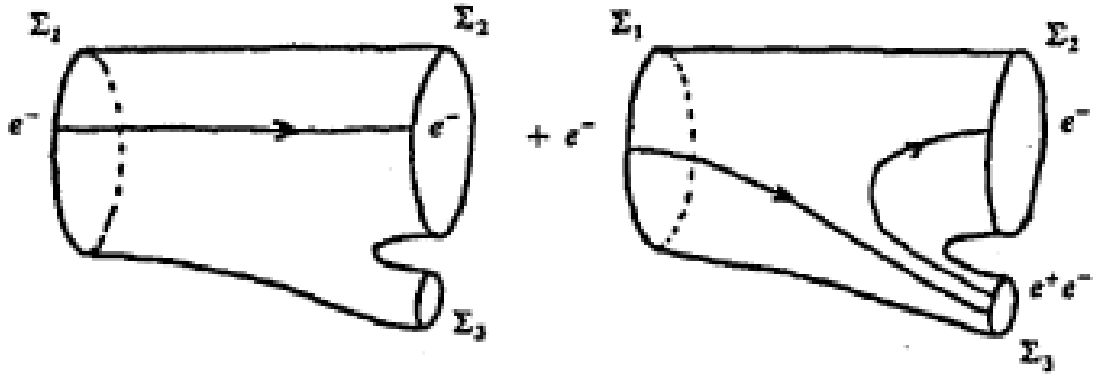

Fig. 2

II. Muon number “non-conservation” process

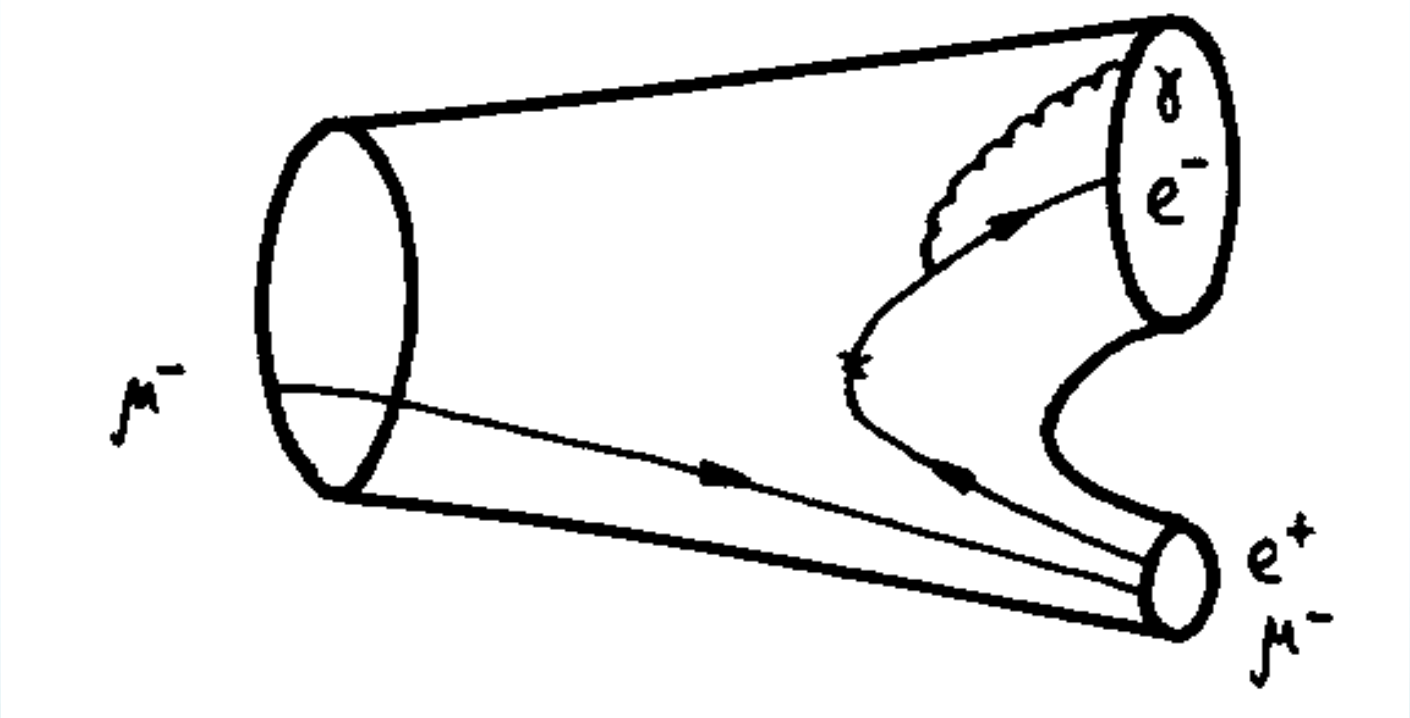

II. Giddings-Strominger axion Wormholes

Giddings-Strominger 1988

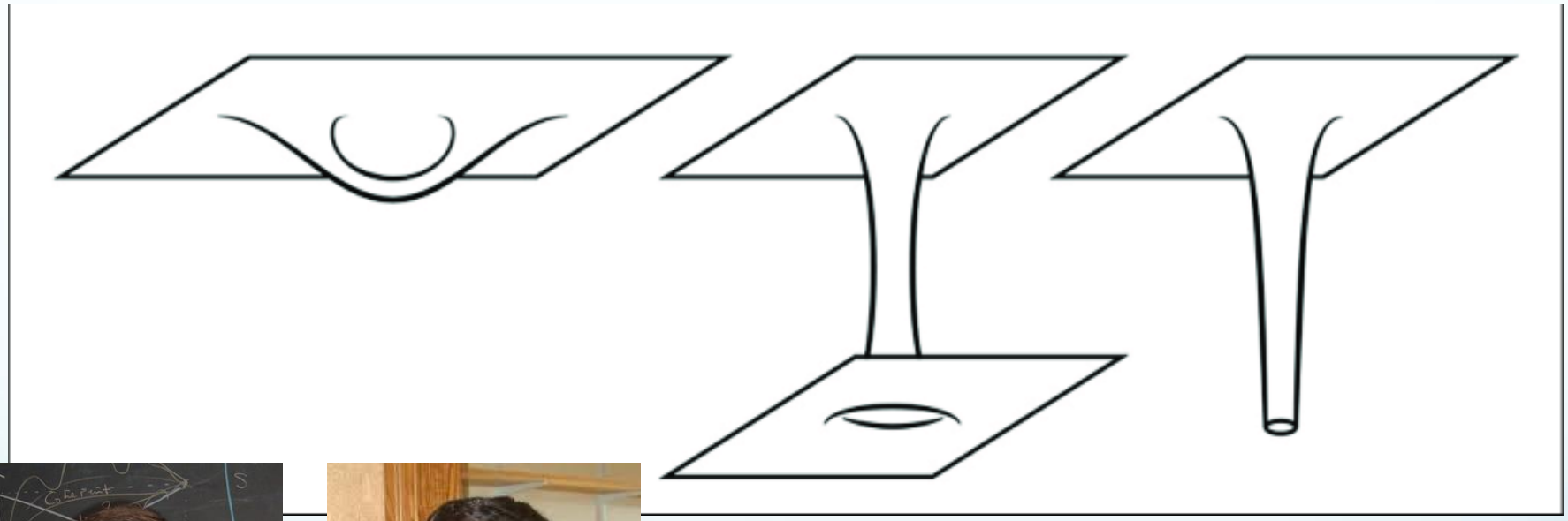

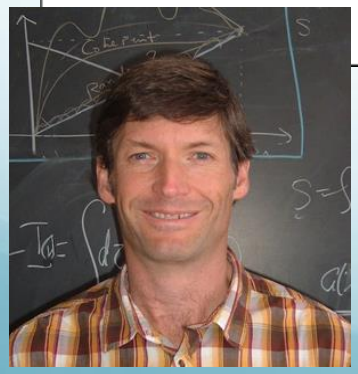

III. Interpretation of Wormholes

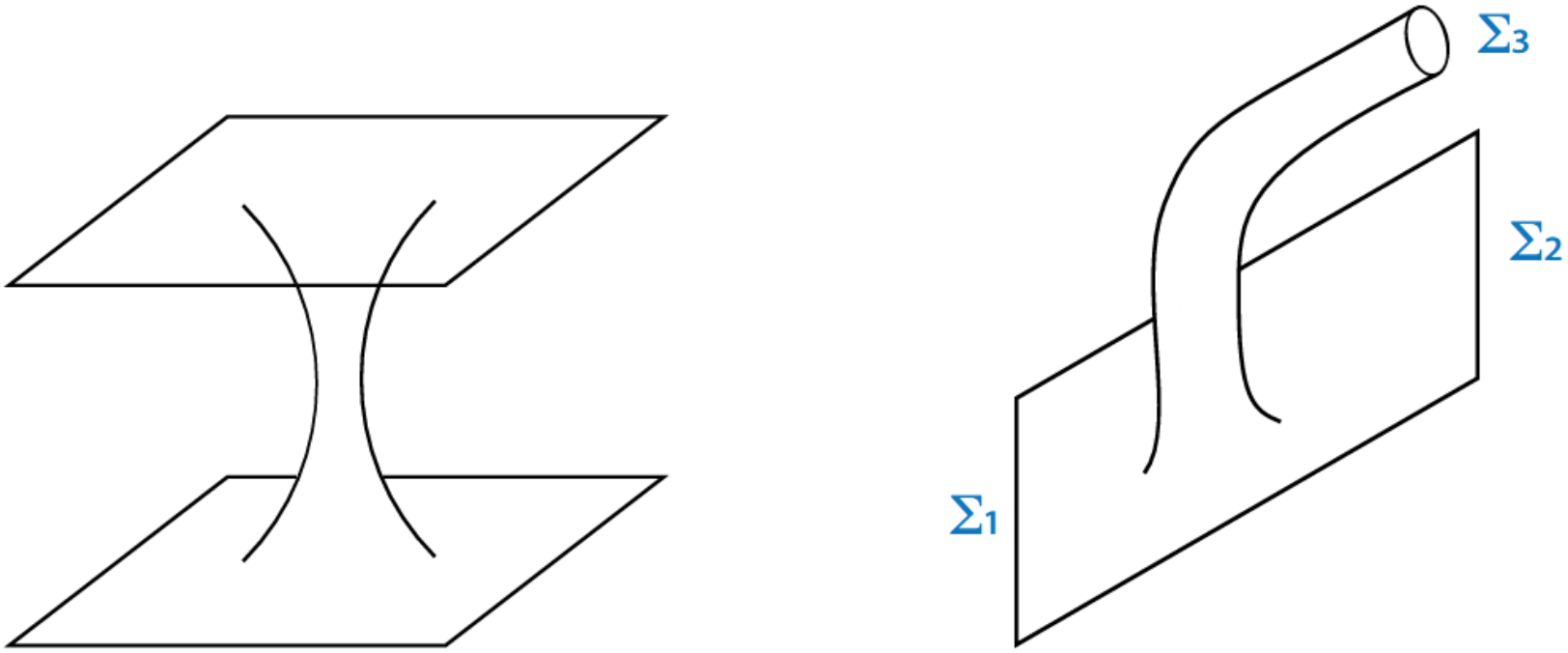

Figure 1: Common interpretations of Euclidean wormholes. On the left, a full wormhole connecting two asymptotic regions. On the right, a semi-wormhole, leading to the creation of a baby universe (Σ_3).

III: Baby universe interpretation

G.L., Rubakov, Tinyakov 1988

Euclidean wormholes can be interpreted as tunnelling events leading to the creation of baby universes [3, 8]. It was noted in [23] that GS wormholes are leading to the materialisation of baby universes which are *contracting* after analytic continuation to Minkowski time. Indeed, a regular wormhole at $\tau = 0$ has finite size $a(0) = a_0 \neq 0$, and zero derivative $\dot{a}(0) = 0$ such that for small τ we can expand

$$a(\tau) = a_0 + \frac{1}{2} a_2 \tau^2 + \mathcal{O}(\tau^4) \,, \tag{14}$$

where the coefficient $a_2 = \ddot{a}(0)$. After analytic continuation to Minkowski time $t = -i\tau$ we get

$$a(t) = a_0 - \frac{1}{2} a_2 t^2 + \mathcal{O}(t^4) \,. \tag{15}$$

Now it is clear that $a_2 > 0$ and $a_2 < 0$ correspond respectively to contracting and expanding small universes. The GS wormhole obviously has $a_2 = \ddot{a}(0) > 0$, since the neck of the wormhole is a minimum of $a(\tau)$. Instead, a wormhole leading to an *expanding* baby universe should have $a_2 = \ddot{a}(0) < 0$, *i.e.* the "neck" of such a wormhole should be a local maximum.

III: Baby universe interpretation

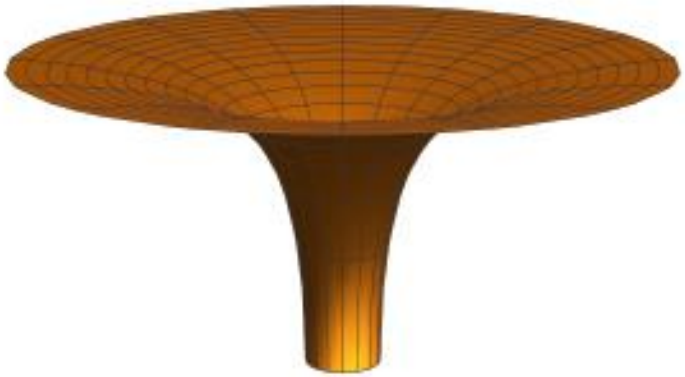

(a) Giddings-Strominger-type wormhole.

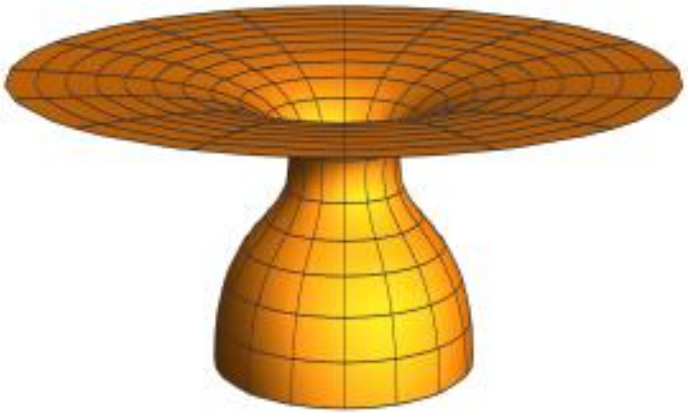

(b) Wormhole leading to an expanding baby universe.

IV. Linear stability analysis:

- **Rubakov & Shvedov 1996,** Found single negative mode about GS wormhole in O(4) symmetric (homogeneous) sector
- **Alonso & Urbano, 2017-2019,** Showed that there are no negative modes in homogeneous sector!
- **Hertog, Truijen & VanRiet, 2019,** Clamed that Euclidean Axion Wormholes have multiple non-homogeneous Negative Modes
- **Loges, Shiu & Sudhir, 2022,** Using gauge invariant approach showed showed that Euclidean Axion Wormholes do not have any Negative Modes.

2.Setup

Our starting point is the Euclidean action for gravity coupled to an axion and a dilaton/scalar ϕ, which reads [20]:

$$S_{\rm E} = \int {\rm d}^4x\sqrt{g}\left(-\frac{1}{2\kappa}R + \frac{1}{2}\nabla_\mu\phi\nabla^\mu\phi + V(\phi) + \frac{1}{12f^2}e^{-\beta\phi\sqrt{\kappa}}H_{\mu\nu\rho}H^{\mu\nu\rho}\right)\,, \tag{1}$$

where $\kappa \equiv M_{\rm Pl}^{-2} = 8\pi G$, the dilatonic coupling constant is denoted β and the potential $V(\phi)$, $H_{\mu\nu\rho}$ being the 3-form field strength of an axion field with coupling f. When $\beta \neq 0$, we refer to ϕ as a dilaton, while for $\beta = 0$ we simply call it a scalar.

We will focus on the following spherically symmetric and homogeneous ansatz

$$\begin{cases} {\rm d}s^2 = h^2(\tau){\rm d}\tau^2 + a(\tau)^2{\rm d}\Omega_3^2\,, \\ \phi = \phi(\tau)\,, \\ H_{0ij} = 0\,,\ H_{ijk} = q\varepsilon_{ijk}\,, \end{cases} \tag{3}$$

On-shell action

Using the trace of the first equation in (2), the on-shell action of the wormhole solution can be easily calculated

$$S_{\rm E} = \int {\rm d}^4x\sqrt{g}\left(\frac{{\rm e}^{-\beta\phi\sqrt{\kappa}}}{6f^2}H^2 - V(\phi)\right) \tag{8}$$

$$= 2\pi^2\int {\rm d}\tau h a^3\left(\frac{2N^2{\rm e}^{-\beta\phi\sqrt{\kappa}}}{a^6} - V(\phi)\right), \qquad N^2 \equiv \frac{q^2}{2f^2} \tag{9}$$

where in the second line we used the spherically symmetric ansatz. Note that this expression for the on-shell action is equivalent to the action (4) upon using the constraint (6) and keeping the surface term. From this expression of the action (9) we can conclude that for some potentials the wormhole action can become negative[1].

Equations of motion

$$\begin{cases} \dfrac{2a\ddot{a}}{h} + \dfrac{\dot{a}^2}{h} - h - \dfrac{2a\dot{a}\dot{h}}{h^2} + \kappa a^2 \left(\dfrac{\dot{\phi}^2}{2h} + hV(\phi) \right) - \dfrac{\kappa N^2 h}{a^4} \mathrm{e}^{-\beta\phi\sqrt{\kappa}} = 0 \,, \\ \dfrac{\dot{a}^2}{h^2} - 1 = \dfrac{\kappa a^2}{3} \left(\dfrac{\dot{\phi}^2}{2h^2} - V(\phi) \right) - \dfrac{\kappa N^2}{3a^4} \mathrm{e}^{-\beta\phi\sqrt{\kappa}} \,, \\ \ddot{\phi} + \left(\dfrac{3\dot{a}}{a} - \dfrac{\dot{h}}{h} \right) \dot{\phi} = h^2 \dfrac{\mathrm{d}V}{\mathrm{d}\phi} - \dfrac{\beta N^2 h^2 \sqrt{\kappa}}{a^6} \mathrm{e}^{-\beta\phi\sqrt{\kappa}} \,. \end{cases} \tag{6}$$

In the gauge $h \equiv 1$, these equations simplify to

$$\begin{cases} 2a\ddot{a} + \dot{a}^2 - 1 + \kappa a^2 \left(\dfrac{\dot{\phi}^2}{2} + V(\phi) \right) - \dfrac{\kappa N^2}{a^4} \mathrm{e}^{-\beta\phi\sqrt{\kappa}} = 0 \,, \\ \dot{a}^2 - 1 = \dfrac{\kappa a^2}{3} \left(\dfrac{\dot{\phi}^2}{2} - V(\phi) \right) - \dfrac{\kappa N^2}{3a^4} \mathrm{e}^{-\beta\phi\sqrt{\kappa}} \,, \\ \ddot{\phi} + \dfrac{3\dot{a}}{a} \dot{\phi} = \dfrac{\mathrm{d}V}{\mathrm{d}\phi} - \dfrac{\beta N^2 \sqrt{\kappa}}{a^6} \mathrm{e}^{-\beta\phi\sqrt{\kappa}} \,. \end{cases} \tag{7}$$

Initial conditions

At the wormhole neck we have $\dot{a}(0) = 0$ and $\dot{\phi}(0) = 0$

and in the asymptotic future $\tau = \tau_f \to \infty$, $\dot{a}(\tau_f) = 1$ and $\dot{\phi}(\tau_f) = 0$.

On the classical solution, we must also specify the initial values of the scale factor and scalar field. The value of the scalar field $\phi(0) = \phi_0$ is a free parameter, while the throat size, $a(0) = a_0$, is determined by the Friedmann constraint at $\tau = 0$:

$$1 = \frac{\kappa}{3}\left(a_0^2 V(\phi_0) + \frac{Q^2}{a_0^4}\right), \tag{17}$$

$$\Leftrightarrow \frac{\kappa}{3}V(\phi_0)x^3 - x^2 + \frac{\kappa Q^2}{3} = 0\,, \quad x = a_0^2\,, \tag{18}$$

where we defined

$$Q^2 = N^2 \mathrm{e}^{-\beta\phi_0\sqrt{\kappa}}\,. \tag{19}$$

The discriminant of the cubic equation (18) is $\Delta = \frac{\kappa Q^2}{2}\left(4 - \kappa^3 Q^2 V(\phi_0)^2\right)$. When $\Delta > 0$, there are three real solutions for x, while when $\Delta < 0$, there are one real and two complex solutions

GS solution

The GS wormhole solution [3] has $V = 0$ and in the gauge $a = \tau$ can be written as [17]

$$a(\tau) = \tau\,, \quad h(\tau) = \left(1 - \frac{a_0^4}{\tau^4}\right)^{-1/2}\,, \quad \mathrm{e}^{\beta\phi(\tau)\sqrt{\kappa}} = \frac{\kappa N^2}{3a_0^4}\cos^2\left[\frac{\beta}{\beta_c}\arccos\left(\frac{a_0^2}{\tau^2}\right)\right], \tag{10}$$

where β_c denotes the critical value of the dilaton coupling above which no solution exists, with

$$a_0^4 = \frac{\kappa N^2}{3}\cos^2\left(\frac{\pi}{2}\frac{\beta}{\beta_c}\right), \qquad 0 \le \beta < \beta_c = \frac{2\sqrt{2}}{\sqrt{3}}\,. \tag{11}$$

The action of this wormhole can be easily calculated and reads

$$S_{GS}^{(\beta)} = 2\pi^2\int_{a_0}^{\infty} \mathrm{d}\tau\, \frac{2N^2\mathrm{e}^{-\beta\phi\sqrt{\kappa}}}{\tau^3\sqrt{1-\frac{a_0^4}{\tau^4}}} = \frac{4\sqrt{2}\pi^2 N}{\beta\sqrt{\kappa}}\sin\left(\frac{\pi}{2}\frac{\beta}{\beta_c}\right). \tag{12}$$

In the limit $\beta \to 0$, one gets a version of the GS solution without dilaton, whose action is

$$S_{GS}^{(0)} = \frac{\sqrt{3}\pi^3 N}{\sqrt{\kappa}}\,. \tag{13}$$

3. Axion-dilaton wormholes

After these preliminaries, we are ready to search for wormhole solutions. We will start with the case of the axion-dilaton-gravity system, where we assume the dilaton to be massive, that is to say we choose the potential

$$V(\phi) = \frac{1}{2} m^2 \phi^2 \,, \tag{26}$$

where m is the dilaton mass. The equations of motion (7) in the gauge $h = 1$ now read

$$\begin{cases} 2a\ddot{a} + \dot{a}^2 - 1 + \kappa a^2 \left(\dfrac{\dot{\phi}^2}{2} + \dfrac{1}{2} m^2 \phi^2 \right) - \dfrac{\kappa N^2}{a^4} \mathrm{e}^{-\beta\phi\sqrt{\kappa}} = 0 \quad \text{(acceleration equation)} \,, \\ \dot{a}^2 - 1 = \dfrac{\kappa a^2}{3} \left(\dfrac{\dot{\phi}^2}{2} - \dfrac{1}{2} m^2 \phi^2 \right) - \dfrac{\kappa N^2}{3a^4} \mathrm{e}^{-\beta\phi\sqrt{\kappa}} \quad \text{(Friedmann constraint)} \,, \\ \ddot{\phi} + \dfrac{3\dot{a}}{a} \dot{\phi} = m^2 \phi - \dfrac{\beta N^2 \sqrt{\kappa}}{a^6} \mathrm{e}^{-\beta\phi\sqrt{\kappa}} \quad \text{(dilaton equation)} \,. \end{cases} \tag{27}$$

"Effective potential"

The dilaton equation in (27) possesses a mechanical analogy as the motion of a *particle* $\phi(\tau)$ in an *effective potential* $W(\phi)$:

$$W(\phi) = -V(\phi) - \frac{N^2}{a^6} \mathrm{e}^{-\beta\phi\sqrt{\kappa}} , \tag{28}$$

$$\frac{\mathrm{d}W(\phi)}{\mathrm{d}\phi} = -m^2\phi + \frac{\beta N^2\sqrt{\kappa}}{a^6} \mathrm{e}^{-\beta\phi\sqrt{\kappa}} . \tag{29}$$

We see that the fate of the particle released at some point $\phi(0) = \phi_0 > 0$ with zero velocity $\dot{\phi}(0) = 0$ depends on the sign of $W_{,\phi}$ at this point. Depending on which term in the potential $W(\phi)$ dominates at this point, the particle either starts to move to the right (increasing ϕ) or to the left (decreasing ϕ). Since we want to obtain an asymptotically flat geometry, for $\tau \to \infty$ the dilaton field should eventually settle at its vacuum value $\phi = 0$. The shape of the effective potential crucially depends on the axion charge N, and also on which root is chosen in (22) – see Fig. 3 for an illustration.

$$F_{\text{friction}} = \frac{3\dot{a}}{a}\dot{\phi} .$$

“Effective potential”

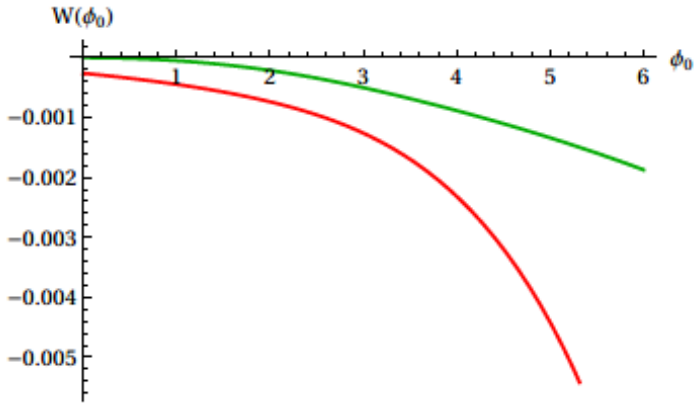

(a) Monotonic effective potential.

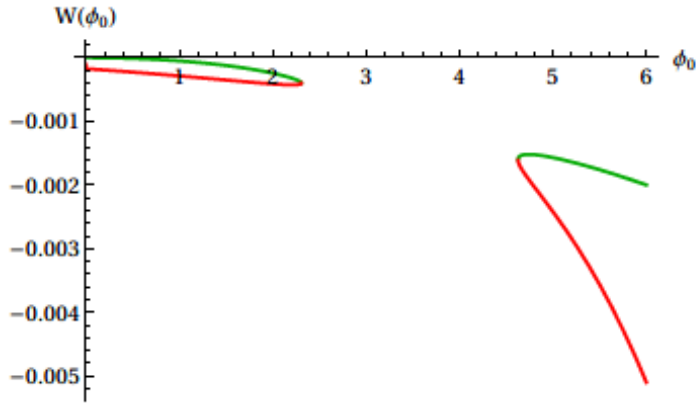

(b) Non-monotonic effective potential.

Figure 3: Effective potential $W(\phi)$ as a function of ϕ_0 for axion charge $N = 20000$ (left) and $N = 30000$ (right). The other parameters are the same for both plots: $m = 0.01$ and $\beta = 1.2$. The green line corresponds to the large root in (22), while the red line corresponds to the smaller positive root. The plot on the right contains a gap, which is caused by there existing no real solutions to the cubic equation (18) in that range.

Generalisations of GS wormholes

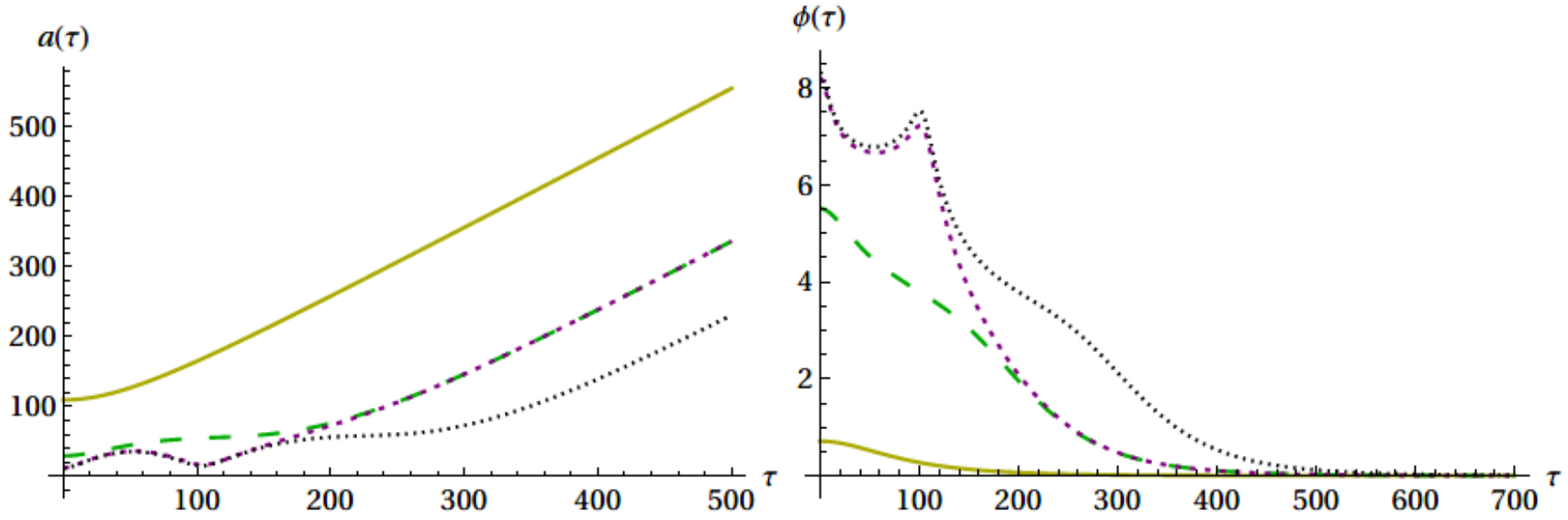

Figure 4: Wormhole solutions with a massive dilaton, with the scale factor shown on the left and the dilaton evolution on the right. All solutions have $\kappa = 1$, $\beta = 1.2$, $N = 30000$, $m = 0.01$. The individual solutions are characterised by the initial value of the dilaton, given respectively by the values $\phi_0 = 0.7118165858, 5.5075291704, 8.1964321797, 8.3116654157$ (we indicate a number of significant digits such that the action can be determined to better than percent level accuracy). Solutions with larger ϕ_0 display a more intricate field evolution, containing oscillations of the fields.

Generalisations of GS wormholes

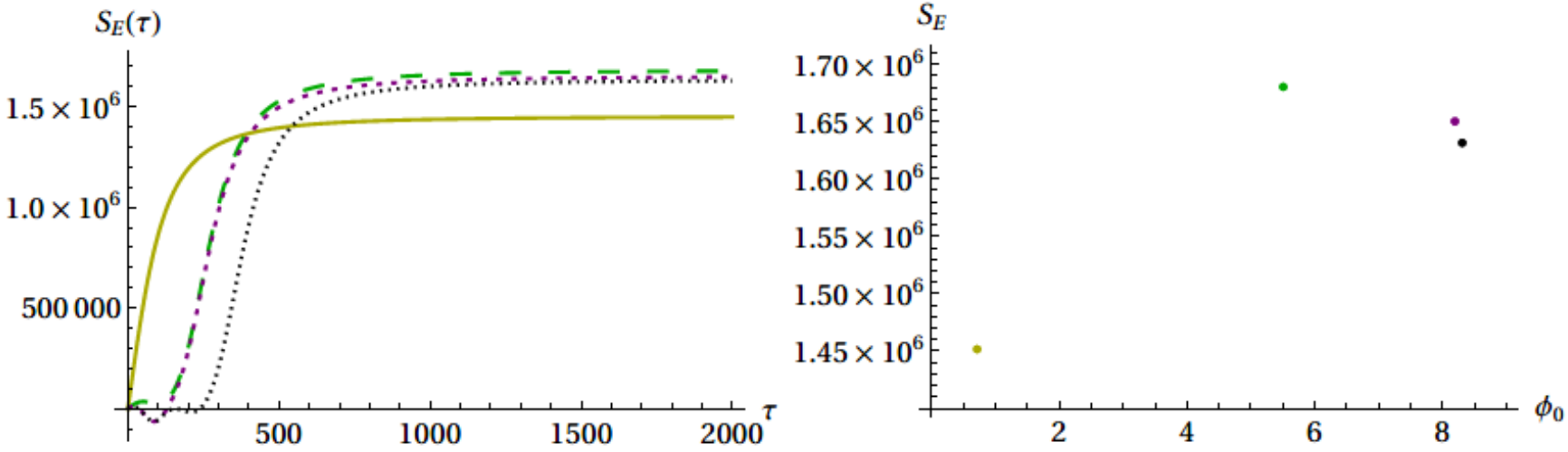

Figure 5: The Euclidean action, as a function of τ (left plot) and a graph with the asymptotic values (right plot), for the solutions shown in Fig. 4. Intriguingly, the action is not monotonic in ϕ_0, but starts decreasing as more oscillations are added.

Generalisations of GS wormholes

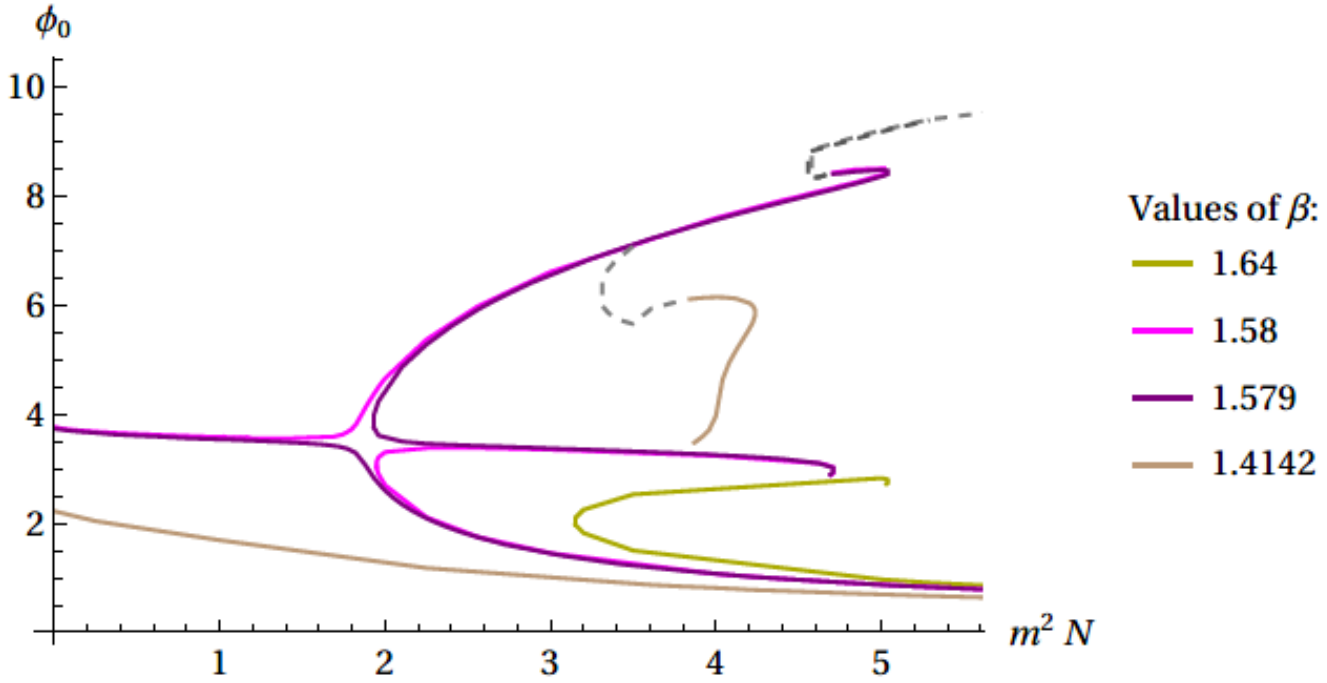

Figure 8: Branch structure of the generalised GS-type solutions with at most one extra minimum of the scale factor, for four representative values of the dilaton coupling. A full description is provided in the main text.

Axion-Dilaton wormholes leading to expanding baby universes

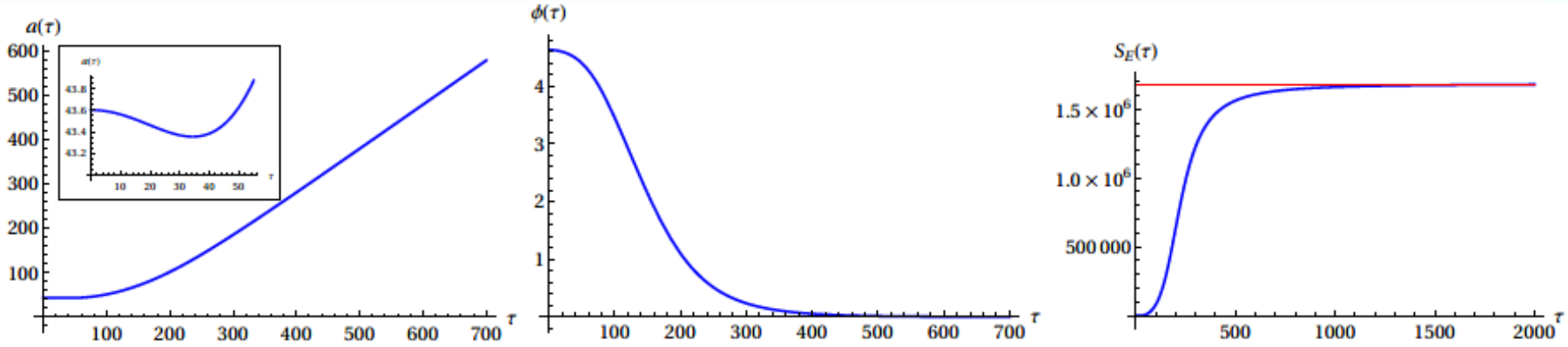

Figure 11: An example of a wormhole leading to an expanding universe upon analytic continuation. For this solution, the dilaton rolls down the potential monotonically. Shown are the scale factor (left), dilaton (middle) and Euclidean action (right). The red line represents the value of the final Euclidean action when taking the analytic remainder into account (see Appendix C). The parameter values are $m = 0.01$, $\beta = 1.2$, $N = 30000$ and the initial dilaton value is $\phi_0 = 4.6297956230$.

Axion-Dilaton wormholes leading to expanding baby universes

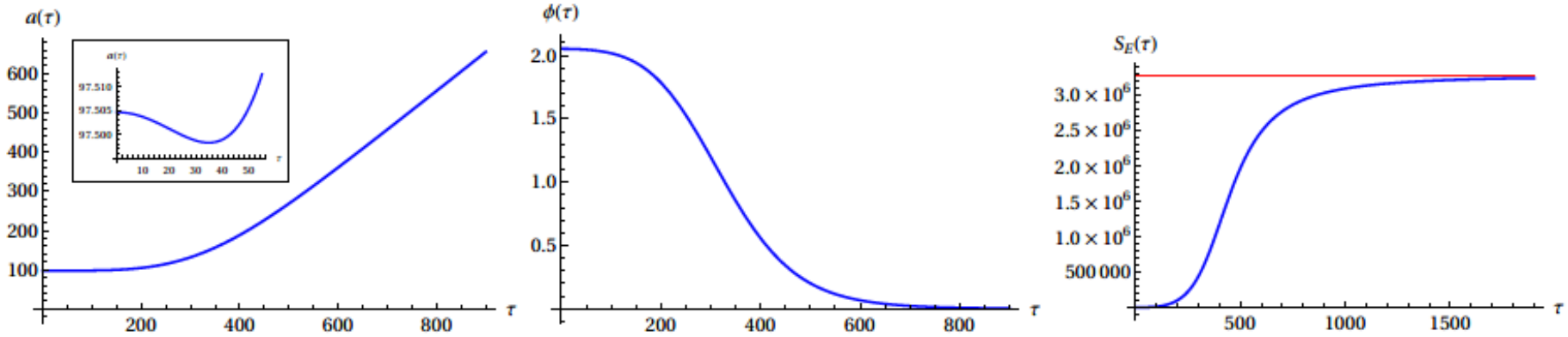

Figure 19: An example of a wormhole with large dilaton coupling, in this case $\beta = 2$. Shown are again the scale factor (left), dilaton (middle) and Euclidean action (right). The parameter values are $m = 0.01$, $\beta = 2$, $N = 73940$ and the initial dilaton value is $\phi_0 = 2.0522333714$.

Axion-Dilaton wormholes leading to expanding baby universes

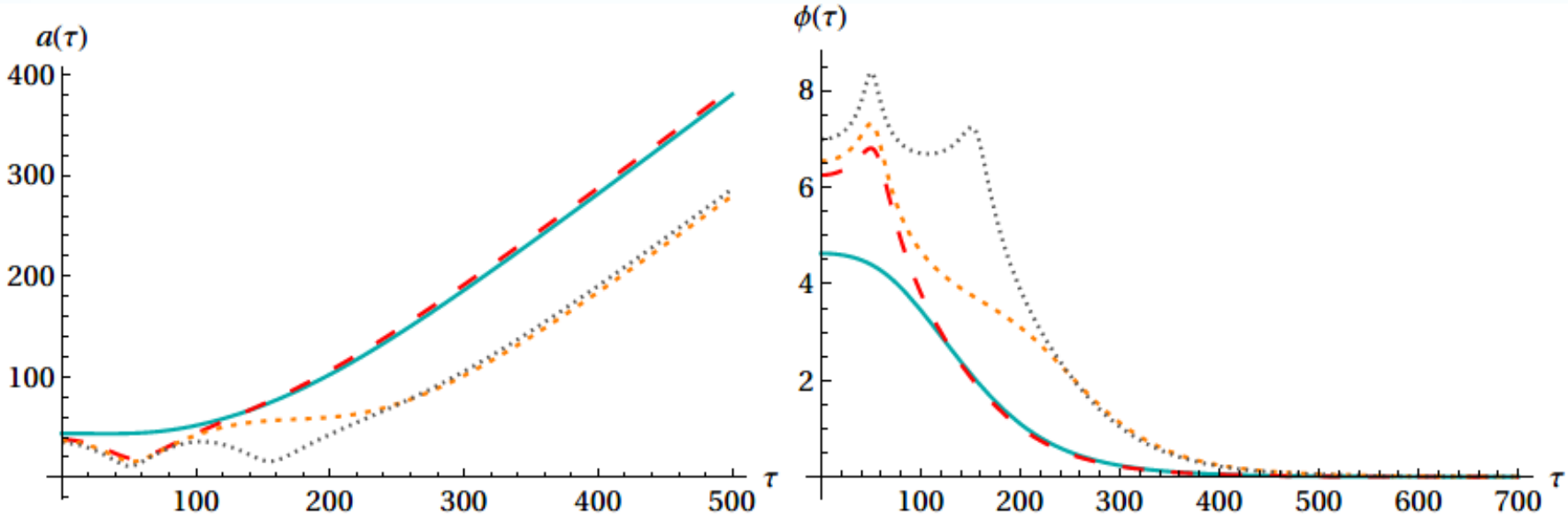

Figure 12: Expanding wormhole solutions with a massive dilaton, with the scale factor shown on the left and the dilaton evolution on the right. All solutions have $\kappa = 1$, $\beta = 1.2$, $N = 30000$, $m = 0.01$. The individual solutions are characterised by the initial value of the dilaton, given respectively by the values $\phi_0 = 4.6297956230, 6.2498081147, 6.5411315634, 6.9914512133$. Solutions with larger ϕ_0 display a more intricate field evolution, containing oscillations of the fields.

Axion-Dilaton wormholes leading to expanding baby universes

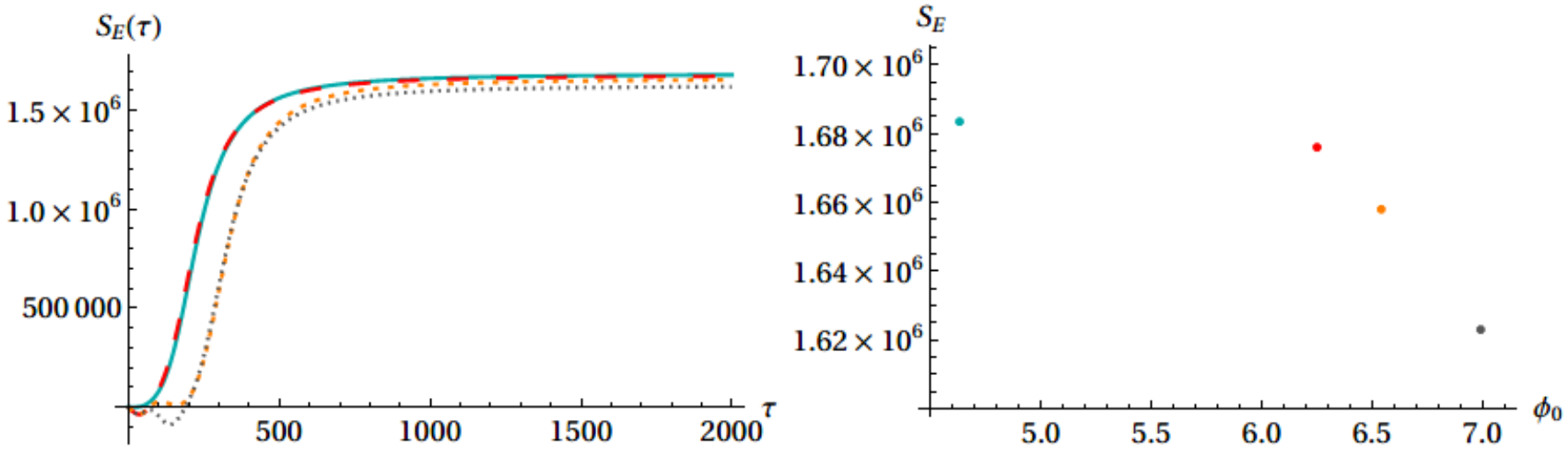

Figure 13: The Euclidean action, as a function of τ (left plot) and a graph with the asymptotic values (right plot), for the solutions shown in Fig. 12. Surprisingly, the action decreases as the field evolutions become more involved.

Comparision of GS and expanding wormholes

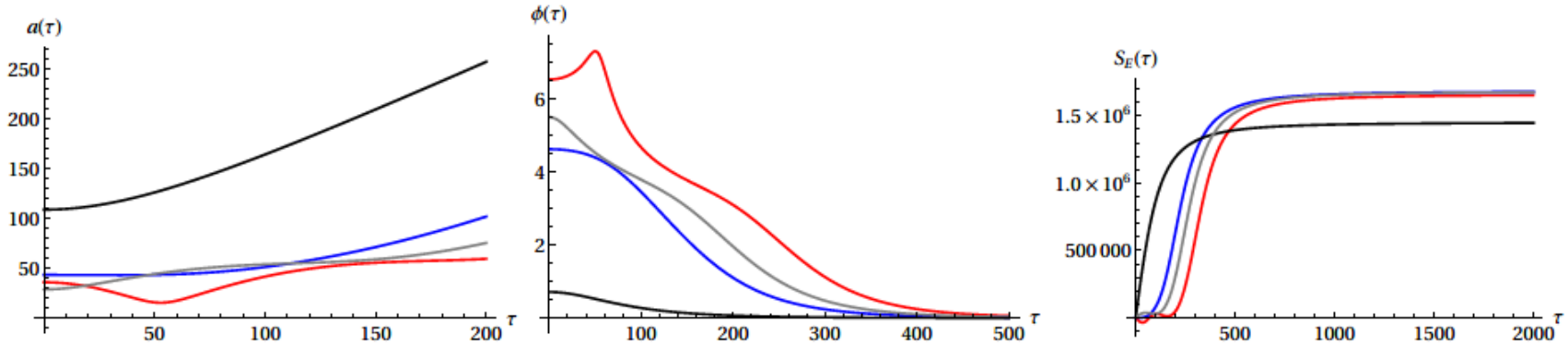

Figure 21: This figure compares GS-type and expanding wormholes, at the same parameter values $m^2N = 3$ and dilaton coupling $\beta = 1.2$. The GS-type solutions are depicted by the black ($\phi_0 \approx 0.7$) and grey ($\phi_0 \approx 5.5$) lines. These solutions were already presented in Fig. 4. The blue ($\phi_0 \approx 4.6$) and red ($\phi_0 \approx 6.2$) curves correspond to expanding wormholes, and were shown in Fig. 12. Interestingly, the actions are seen to be quite close to each other, with the grey solution lying in between the two expanding wormhole solutions. It appears that overall the black GS-type solution is dominant, but a verification of this assertion would require an understanding of the infinite oscillation limit of expanding wormholes.

4. Axion-scalar wormholes leading to expanding baby universes

We will choose the scalar field potential to be of double well form

$$V(\phi) = \frac{1}{4}\lambda(\phi^2 - v^2)^2 \,,$$

where λ is a dimensionless scalar field self-coupling and v is the vacuum expectation value

The equations of motion (7) then read

$$\begin{cases} 2a\ddot{a} + \dot{a}^2 - 1 + \kappa a^2 \left(\dfrac{\dot{\phi}^2}{2} + V(\phi) \right) - \dfrac{\kappa N^2}{a^4} = 0 \quad \text{(acceleration equation)} \,, \\ \dot{a}^2 - 1 = \dfrac{\kappa a^2}{3} \left(\dfrac{\dot{\phi}^2}{2} - V(\phi) \right) - \dfrac{\kappa N^2}{3a^4} \quad \text{(Friedmann constraint)} \,, \\ \ddot{\phi} + \dfrac{3\dot{a}}{a}\dot{\phi} = \dfrac{\mathrm{d}V}{\mathrm{d}\phi} \quad \text{(scalar equation)} \,. \end{cases}$$

Axion-scalar wormholes leading to expanding baby universes: Large charge case

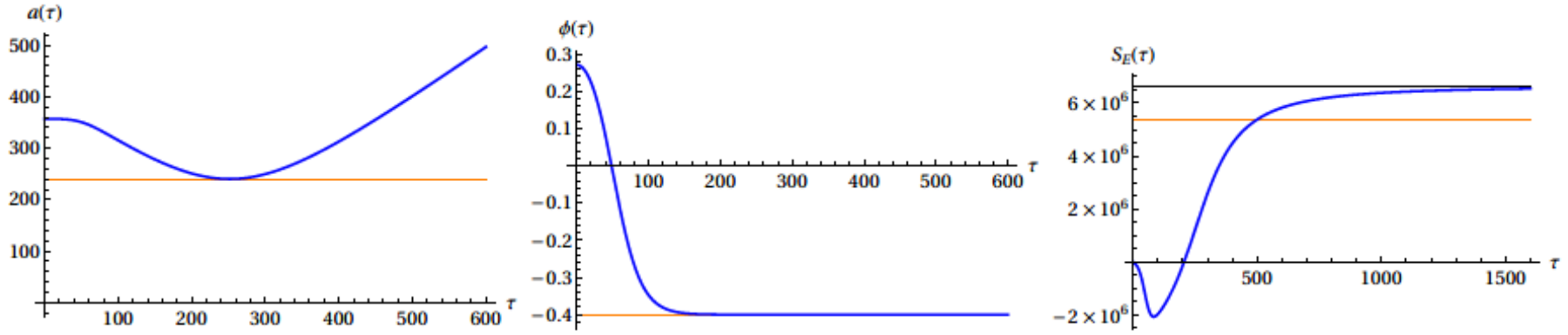

Figure 23: An example of an expanding wormhole supported by a large axionic charge, and a scalar field in a double well potential. The parameters used are $\lambda = 0.01$, $N = 100000$, $v = 0.4$. The initial scalar field value is $\phi_0 = 0.27112946714882599307$. The orange lines provide the GS wormhole values as reference.

Axion-scalar wormholes leading to expanding baby universes: Small charge case

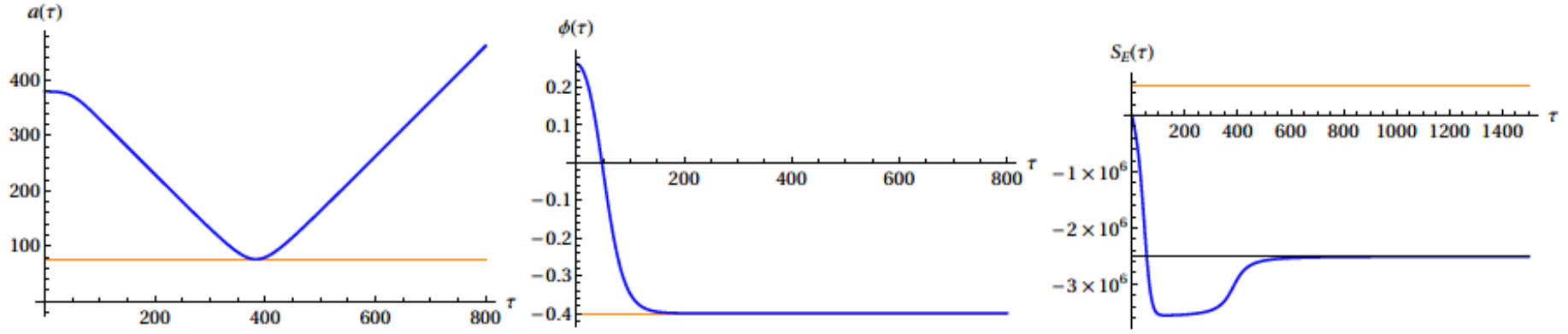

Figure 24: An example of an expanding wormhole supported by a small axionic charge. The parameters used are $\lambda = 0.01$, $N = 1000$, $v = 0.4$. The initial scalar field values is $\phi_0 = 0.26235021388116072967$.

Axion-scalar wormholes leading to expanding baby universes: Action vs N

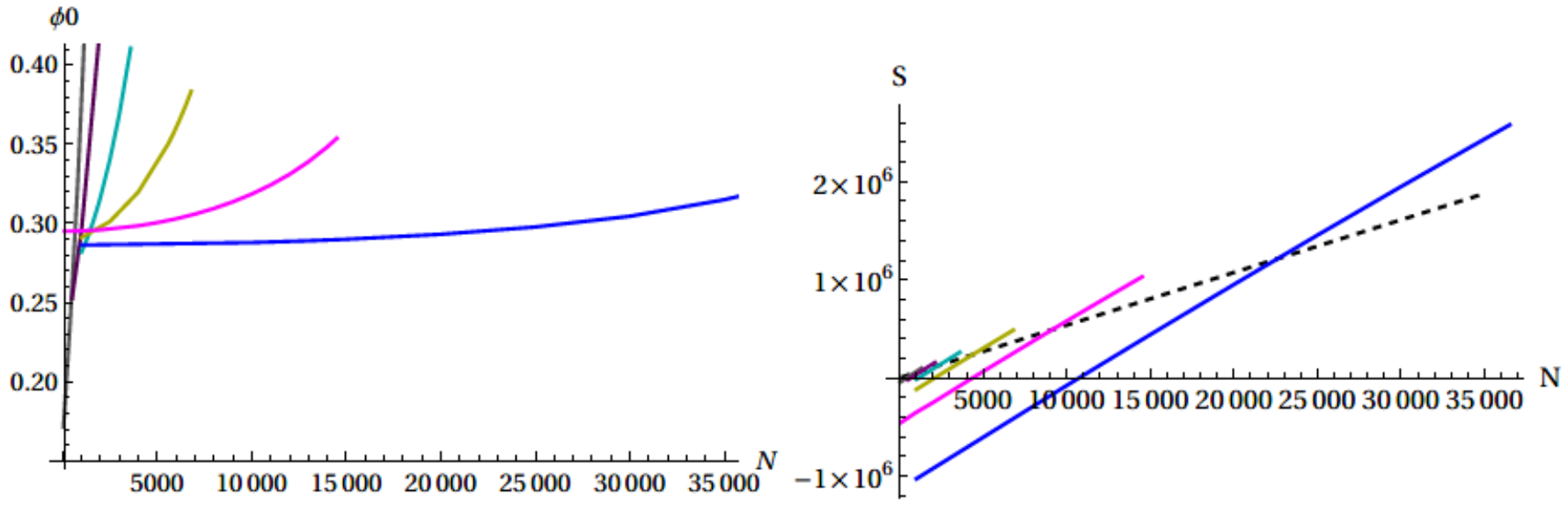

Figure 28: Summary plots for $v = 1.0$ (black), $v = 0.9$ (purple), $v = 0.8$ (turquoise), $v = 0.7$ (green), $v = 0.6$ (pink) and $v = 0.5$ (blue). Here $\lambda = 0.01$. The right plot shows the most striking result, namely that the action varies linearly with the charge N. For small enough charge, the action becomes negative. The dashed black line is the Giddings-Strominger value of the action.

Axion-scalar wormholes leading to expanding baby universes: Action to charge ratio

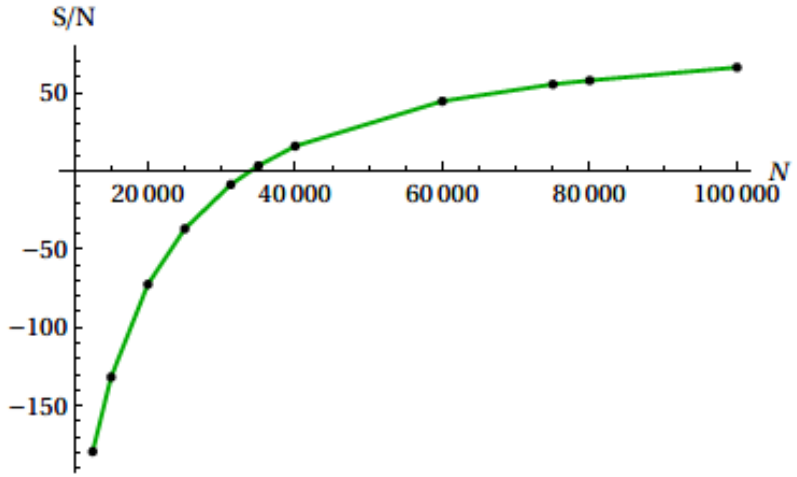

(a) $v = 0.4$

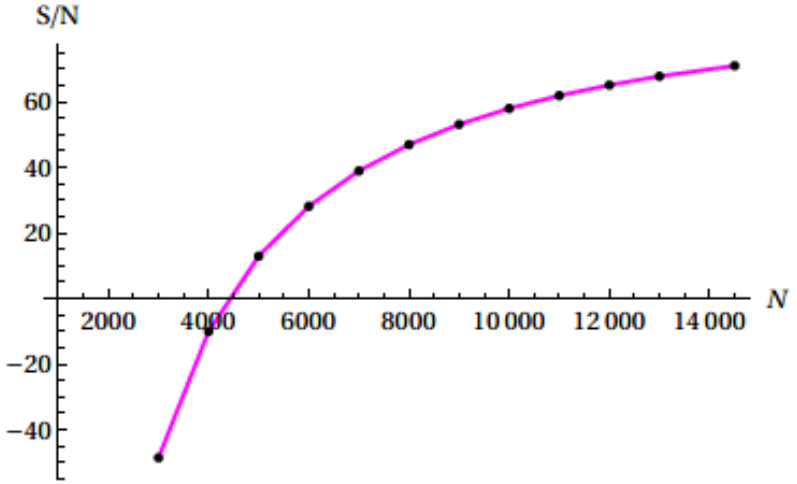

(b) $v = 0.6$

Figure 26: Plots of the action-to-charge ratio for $v = 0.4$ (left) and $v = 0.6$ (right) with $\lambda = 0.01$.

Oscillating Axion-scalar wormholes

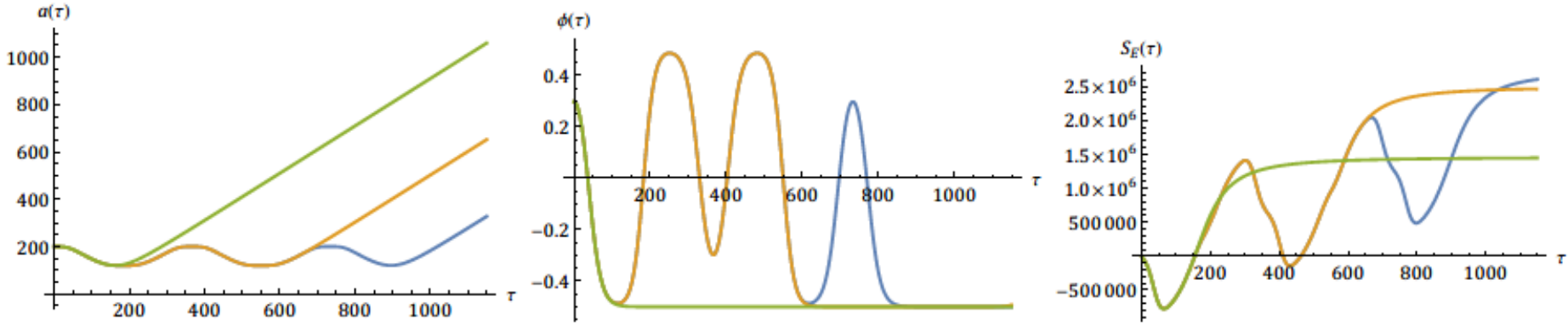

Figure 27: Comparison of solutions with one, two and three minima for the same theory parameters $N = 25000$, $\lambda = 0.01$ and $v = 0.5$. The Euclidean action grows with each additional oscillation. The solutions here are specified by initial scalar field values that lie very close to each other, respectively at $\phi_0 = 0.29769598017296931741454 0$, $0.29753040978542151754655 8$, $0.29753040964664825193709 1$ (these solutions must be optimised to high accuracy in order to determine the action reliably).

Oscillating wormholes

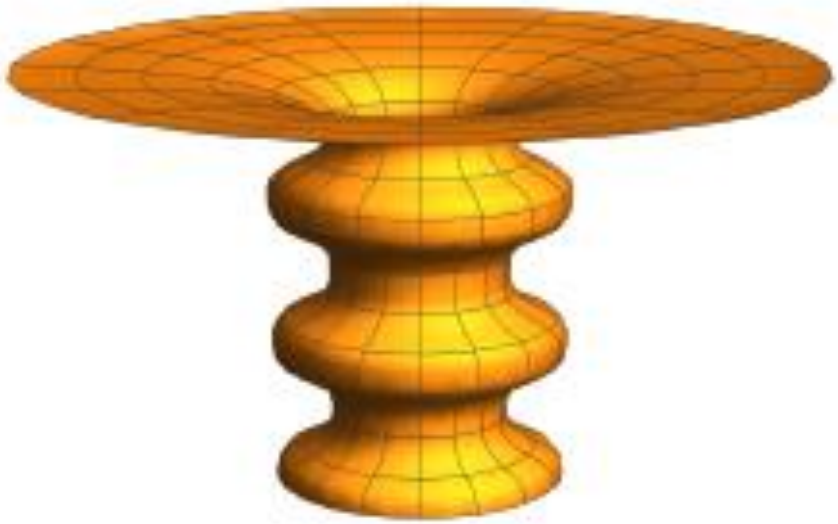

(c) An oscillating wormhole leading to an expanding baby universe.

5. Urgent Open question:

- **Linear stability analysis of various wormhole solutions!**

5. Conclusions :

- **We found a whole zoo of Euclidean axionic wormholes in two different theories: axion - massive dilaton and axion - scalar with a symmetric potential.**
- **Euclidean wormholes are very interesting & exciting, but the same time very confusing & obscure objects.**
- **Definitely more work needs to be done to understand deeply the role of wormholes in quantum gravity and their relevance to physical effects.**

Thanks for attention!

Research supported by

GRMP
Georgia's Researchers' Mobility Programme

Georgia's Researchers Mobility Grant

SRNSFG

Shota Rustaveli National Science Foundation of Georgia Grant FR 21-860

IV. Interpretation of Wormholes:

Three types of solutions

van Riet (2020)

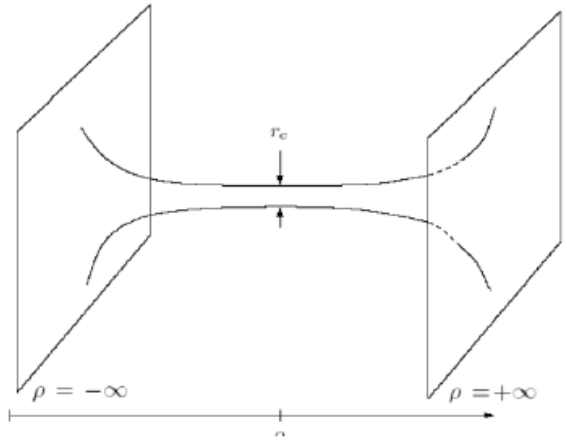

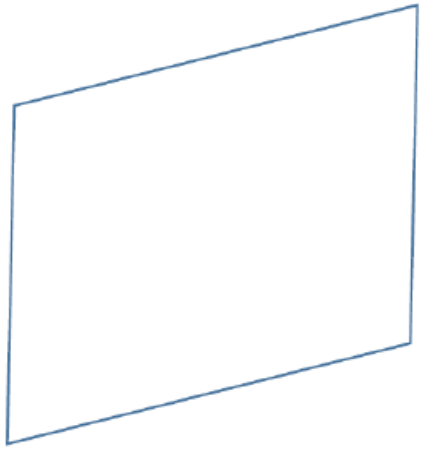

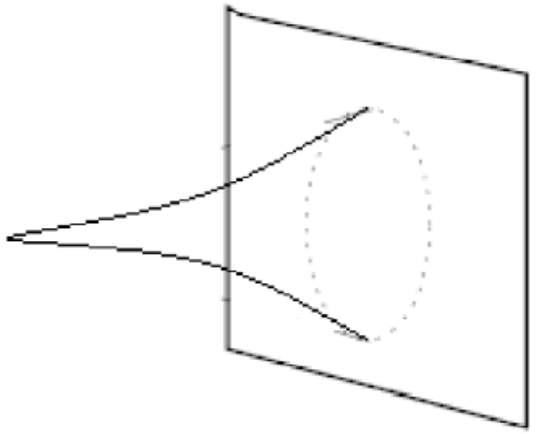

No axion-scalar wormholes with non-trivial scalar field in symmetric potential!

Note also that in the symmetric potential Eq. (32) no GS-type wormholes exist with *non-trivial* scalar field. This conclusion can be easily reached by noting that GS-type wormholes have positive $\dot{a}$, and consequently provide friction in the scalar field equation. So, in order for the solution to end up on one of the hills (vacua) for $\tau \to \infty$ one should start rolling down from higher hill, in order to overcome friction, but in a symmetric potential there is no higher hill. We conclude that the only known GS wormholes in this potential arise with a trivial scalar field configuration $\phi = \pm v$.

Parameter count:

Massive dilaton: N, m, ß; Scalar field: N, λ, v

Under the following rescaling of the fields

$$\phi \to \frac{\phi}{\sqrt{\kappa}}\,,\ a \to \frac{a}{\mu}\,,\ h \to \frac{h}{\mu} \tag{B1}$$

and of the coupling constants to dimensionless variables

$$q \to \frac{q}{\mu^2\sqrt{\kappa}}\,,\ m \to \mu m\,,\ v \to \frac{v}{\sqrt{\kappa}}\,,\ \lambda \to \mu^2\kappa\lambda\,, \tag{B2}$$

the dependance on μ and κ is removed from the equations of motion and the action scales as

$$S \to \frac{1}{\kappa\mu^2}S = \frac{1}{\mu^2/M_{\rm Pl}^2}S\,, \tag{B3}$$

where μ is an arbitrary mass scale. In practice, while searching for solutions this scaling freedom allows us to fix one parameter (*e.g.* m or N in the first theory and λ or N in the second theory) and vary the rest.

Generalisations of GS wormholes

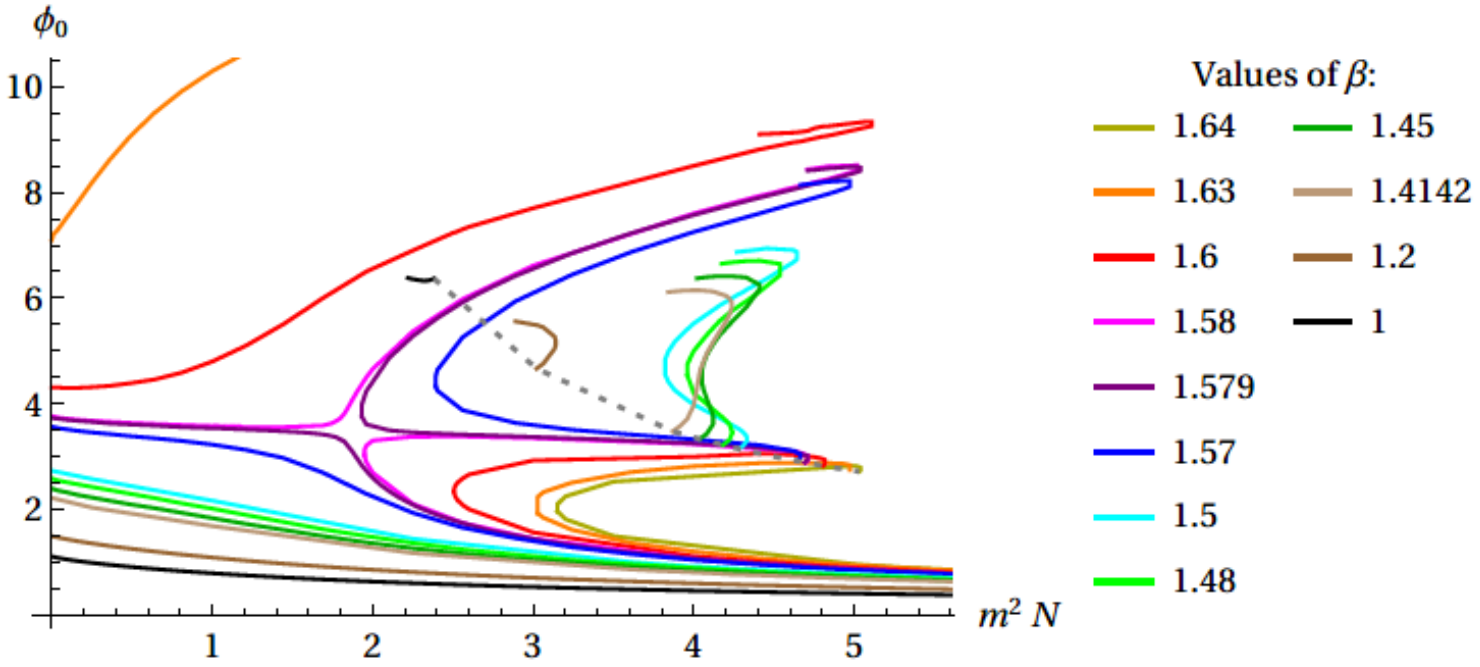

Figure 9: A more complete version of the plot shown in Fig. 8, containing curves at additional values of the dilaton coupling β. The inversion of the branch structure above β_i (*i.e.* for the curves with $\beta \geq 1.58$) is clearly visible. See the main text for a detailed analysis.

Symmetric double well

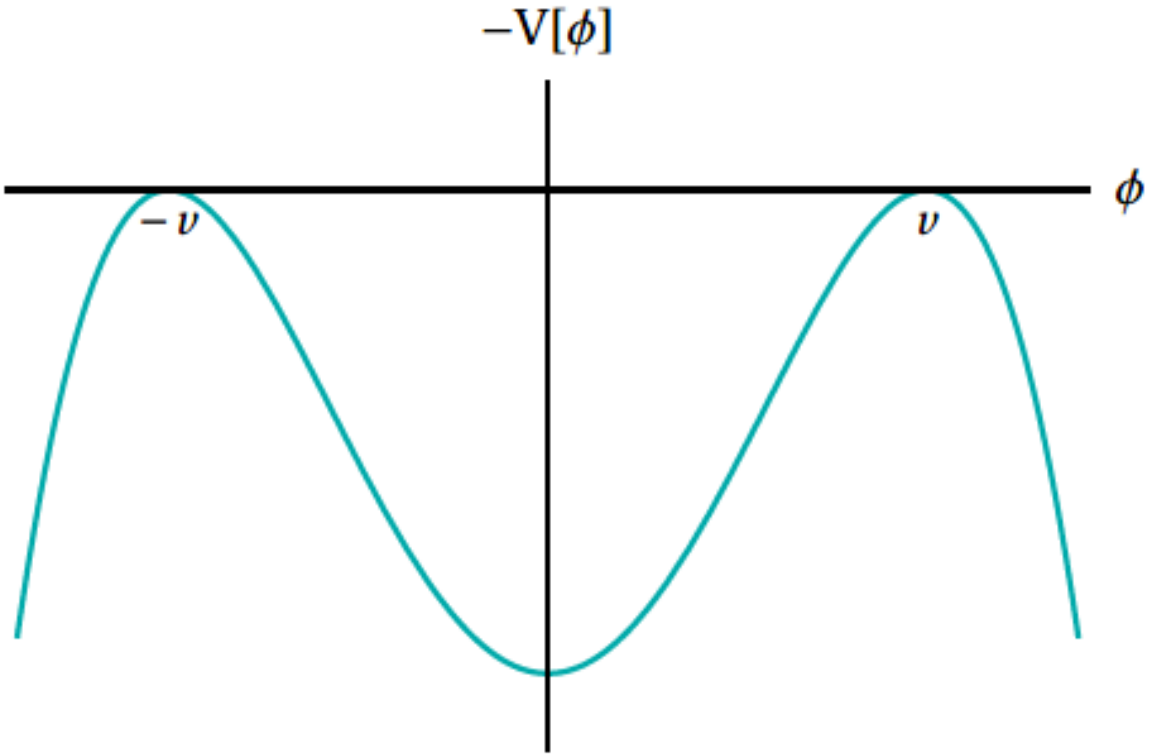

Symmetric double well potential for the parameter values $\lambda = 0.01$ and $v = 0.4$.